Global and Planetary Change 246 (2025) 104722

Contents lists available at ScienceDirect

Global and Planetary Change

journal homepage: www.elsevier.com/locate/gloplacha

Research Article

# Permian thermal pulse event in Southwestern China and its resource and environment effects

Qianqian Feng [a,b], Nansheng Qiu [a,b,c,*], Xiongdong Fu [d], Tenger Borjigin [e], Qingyong Luo [a,b,c], Chuanqing Zhu [a,b,c]

[a] National Key Laboratory of Petroleum Resources and Engineering, China University of Petroleum, Beijing 102249, China
[b] College of Carbon Neutral Energy, China University of Petroleum, Beijing 102249, China
[c] College of Geosciences, China University of Petroleum, Beijing 102249, China
[d] PetroChina Hangzhou Research Institute of Geology, Hangzhou 310023, China
[e] Oil and Gas Survey Center of China Geological Survey, Beijing 100083, China

ARTICLE INFO

Editor: Maoyan Zhu

ABSTRACT

The Emeishan large igneous province (LIP) in Southwestern China and Northern Vietnam is thought to have been a potential driver for the biotic crises and paleoclimatic changes at the Guadalupian-Lopingian boundary (GLB; Permian). Here, we revealed the thermal pulse event induced by the Emeishan LIP and its impact on the fossil energy formation and episodic carbon changes. Southwestern China experienced a pulsating high thermal anomaly lasting 10 Myrs in the mid-Permian, which accelerated the maturation of source rocks, producing mass high-temperature methane emissions. The Emeishan LIP caused large amounts of gases and volcanic ash emissions, which affected the Lopingain organic carbon enrichment. $CO_2$ degassing type changed as the LIP emplacement evolved and the transition from a thermogenic $CO_2$ source to the volcanic carbon source may contribute to two episodes of carbon isotope changes.

## 1. Introduction

Large igneous province (LIP), the product of massive magmatic events, is significantly affected the regional thermal regime, fossil energy formation, ore genesis, and climate crises that triggered mass extinctions in Earth's history. As the Permian large-scale volcanic activity, the Emeishan LIP consists of mafic lava, volcanic clastic rock and igneous rock intrusion, covering an area of $3 \times 10^5$ $km^2$(Xu et al., 2004). Geochronological studies show that the Emeishan LIP was emplaced in a main pulse of ~4 Myrs from 261 Ma to 257 Ma (Huang et al., 2022; Jiang et al., 2023; Shellnutt et al., 2020). The paleontological fossils and the calcium, oxygen, sulfur, carbon isotope records provide evidences for the Guadalupian-Lopingian boundary (GLB; Permian) mass extinction and climate deterioration (Ganino and Arndt, 2009; Jost et al., 2014; Wang et al., 2020; Wignall et al., 2009; Zhang et al., 2015). The Emeishan LIP is proposed as a potential driver of the GLB mass extinction (Huang et al., 2022; Ganino and Arndt, 2009; Wignall et al., 2009; Yang et al., 2018), by the emission of particulates and gasses (i.e., $CO_2$, $SO_2$, $CH_4$) from a magmatic source(Chen et al., 2022; Self et al., 2008), contact metamorphism of sediments(Svensen et al., 2004; Wu et al., 2023), volcanic ash, and widespread wildfires(Grasby et al., 2011; Shen et al., 2011). However, the carbon isotope records present two episodes of the negative excursion across the GLB. The dynamic process driving the episodic carbon changes is not clear. LIPs can result in a high geothermal regime in a short duration. The thermal histories suggested the thermal effect of the Emeishan LIP was sustained for nearly 100 Mys (Qiu et al., 2022), whereas mantle plume models showed the effect lasting for <10 Mys (He, 2022). The duration of thermal event is controversial.

Hydrothermal activity and enhanced heating by the LIP may have caused the deposited oil and gas source rocks to mature rapidly and even lose their hydrocarbon generation capacity. In addition, volcanic eruptions and LIPs changed the atmosphere and hydrosphere, affecting the biosphere evolution, biodiversity and sedimentary environment, influencing the organic matter abundance of the source rock. If the Emeishan LIP affected the GLB paleoclimate, did it influence the distribution and enrichment of organic matter in the Lopingain? Will the hydrothermal activity of Emeishan LIP on the maturation of source rocks and promote

* Corresponding author at: National Key Laboratory of Petroleum Resources and Engineering, China University of Petroleum, Beijing 102249, China.
*E-mail address:* qiunsh@cup.edu.cn (N. Qiu).

https://doi.org/10.1016/j.gloplacha.2025.104722
Received 18 September 2024; Received in revised form 20 January 2025; Accepted 20 January 2025
Available online 21 January 2025

the GLB climate crises? In this study, we reconstructed the thermal history and revealed the thermal pulse event using thermal indicators (vitrinite reflectance, fission track and (U-Th)/He). We identified that the Emeishan LIP acted as a widespread-impact 'coking furnace' for the enrichment and maturation of source rock, and fossil energy formation. We report geothermic evidence to constrain the feedback of LIP to carbon-climate changes.

## 2. Geological setting

The Emeishan LIP is located in South China and northern Vietnam. During the Permian and Triassic , the Laurasian and Gondwanan continents were connected, collectively encircling the Tethys Ocean. The South China block was positioned slightly south of the equator (Huang et al., 2018). The current position of the Emeishan LIP has moved more than 3000 km from its original location. From the Carboniferous to the late Permian, the South China block continuously moved northward from ~10°S to ~10°N by the end Permian. The Permian Pacific mantle plume transited through the South China block (Fig. 1a), leading to crustal uplift and lithospheric thinning due to the ascent of mantle magma. This ascent of the mantle plume, facilitated by regional large fractures and faults, resulted in widespread magmatic eruptions and overflow in South China, forming the Emeishan LIP (Jerram et al., 2016).

The Sichuan Basin (~260,000 km2), adjacent to the Emeishan LIP (Fig. 1b), is a crucial fossil energy production area in China and has significant oil and gas potential. The global paleogeographic map during the end-Guadalupian (Huang et al., 2018) shows that the South China plate was located south of the equator, and the Sichuan Basin was located on the mantle plume formation zone (Fig. 1a). The Emeishan LIP is partly occupied by the Sichuan Basin and its magmas from the Emeishan mantle plume have intruded through sedimentary sequences (Fig. 1d). Large basaltic eruptions, crustal melting, hydrothermal activity, and anomalous heating events occurred in the basin and may have initially covered >500,000 km2 from the inner to the outer zones (Ganino and Arndt, 2009; He et al., 2003). Emeishan basalt is widely distributed in the Sichuan Basin, with a thickness exceeding 300 m in the southwestern part (Fig. 1c).

The formations developed in the Sichuan Basin can be divided into two sedimentary systems: the lower marine carbonate sedimentary from the Sinian to the Middle Triassic and the upper continental clastic sedimentary from the upper Triassic to the Eocene (Fig. 1d). Substantial amounts of pyrobitumen and natural gas pools have been discovered within the Sinian-Cambrian dolostones in the basin. Several sets of hydrocarbon resource rocks developed in the basin. The Cambrian Qiongzhusi Formation, Silurian Longmaxi Formation, and Permian are the dominant source rocks. The geological and geochemical characteristics of these source rocks are shown in the Table 1.

## 3. Materials and methods

### 3.1. Samples

Due to the easy separation of apatite and zircon in sandstones, three sandstone samples, for fission track and U-Th/He analysis, were collected from the Lower Cambrian, Lower Ordovician, and Middle Jurassic strata of the Well YF1 in the intermediate zone of Emeishan LIP. The details of the samples are listed in the Table 2. By reconstructing the temperature evolution of samples at different depths, paleogeothermal gradients, paleoheat flow and land surface temperature can be calculated.

### 3.2. Fission track

Fission track analysis was carried out at the thermochronology laboratory at China University of Petroleum, Beijing. The zircon fission track (ZFT) ages were determined using the external detector method and ζ(zeta) calibration(Hurford and Green, 1983). The apatite fission track (AFT) ages were determined by laser ablation-inductively coupled plasma-mass spectrometry (LA-ICP-MS) method, and calculated by the zeta calibration method(Cogné et al., 2020). The analytical procedures are detailed in the SI Appendix. The data used in this study are reported in Tables 3 and 4.

### 3.3. (U-Th)/He

Zircon (U-Th)/He (ZHe) analysis was conducted at the University of Melbourne, and apatite (U-Th)/He (AHe) analysis was performed at the University of Florida. The details of the analytical procedures are available in the SI Appendix. Data used in this study are summarized in Tables 5 and 6.

### 3.4. Total organic carbon

Total organic carbon (TOC) contents of the core samples were measured at the Wuxi Research Institute of Petroleum Geology, China. The details of the analytical procedures are described in the SI Appendix. Data used in this study are reported in Supplementary Table 1.

### 3.5. Thermal history modeling

The thermal histories were reconstructed using thermal indicators, including the vitrinite reflectance (Ro), AFT, ZFT, AHe, and ZHe data. We used the Easy%$R_o$ model of $R_o$(Sweeney and Burnham, 1990), the multi-kinetic annealing model(Ketcham et al., 2007) of the AFT length and ages, the parallel curvilinear model(Yamada et al., 2007) of the ZFT ages, the radiation damage accumulation and annealing models of the AHe data(Flowers et al., 2009), and ZHe data(Guenthner et al., 2013) for thermal history reconstruction. The HeFTy software with the Monte Carlo approach and the Thermodel for Windows were used. A temperature path was regarded as the effective thermal history of a sample when the difference between the calculated and measured thermal indicator values reached the minimum. The paleothermal gradient ($G_t$) was calculated from the modeled paleotemperatures ($T_1$, $T_2$) and the corresponding paleo-burial depths ($Z_1$, $Z_2$) of different depth samples ($G_t = (T_1\text{-}T_2)/(Z_1\text{-}Z_2)$). The paleo-heat flow values (q) were modeled using $G_t$ and thermal conductivities (K) of the individual strata ($q = G_t \times K$).

### 3.6. Maturity evolution

The temperature and maturity evolution of the source rocks were reconstructed using the Easy%Ro model(Sweeney and Burnham, 1990) with the BasinMod 1D software. The EASY%Ro chemical kinetic model (Sweeney and Burnham, 1990) has been widely used for reconstructing the thermal histories of sedimentary basins, determining the maturity evolution of source rocks, and identifying the hydrocarbon generation stages. The objective of the simulation was to restore the accurate burial history and select appropriate models. The burial and thermal histories of well YF1 were reconstructed by basin modeling using the Ro, and the denudation and thermal histories were derived from the indicators. A transient heat flow model was used for the geothermal calculations, and the model and thermal conductivity were corrected. The burial history was reconstructed using basin modeling. The well completion report of the SINOPEC Exploration Company provides the thickness, top depth, and average lithologies of the well. According to these parameters, the temperature and maturity evolution was corrected by the constrains of vitrinite reflectance and present temperature.

## 4. Geothermic records of Permian thermal pulse event

A linear function relationship exists between temperature, organic

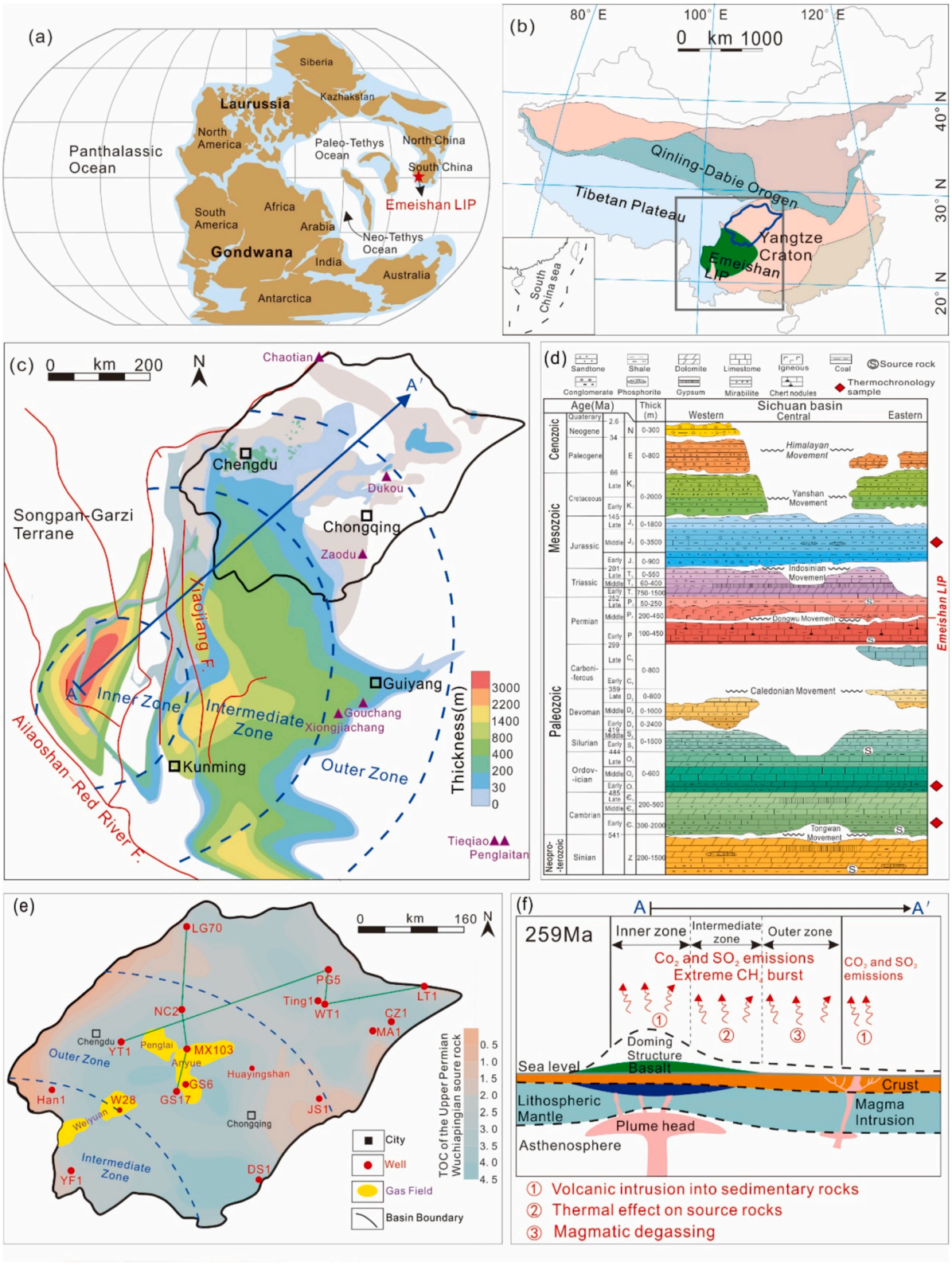


**Fig. 1.** Tectonic and stratigraphic background of the study area. (a) Global paleogeographic map in the end-Guadalupian(Huang et al., 2018) and the locations of South China and Emeishan LIP. (b) Geographic distribution of the Emeishan LIP and Sichuan Basin. (c) Thickness of the Permian basalt. The boundaries of the inner, intermediate, and outer zones in the Emeishan LIP(He et al., 2003) are shown in the blue. The purple triangles represent the carbon isotope profiles for the GLB. (d) Stratigraphic column. The diamonds represent the thermochronology samples. (e) TOC distribution in the Late Permian Wuchiapingian source rock of the Sichuan Basin. (f) Surface uplift, generation of Emeishan basalts, and crustal occurring during the upwelling of the mantle plume(Xu et al., 2004), and greenhouse gas emission patterns (modified after Chen et al., 2022). (For interpretation of the references to colour in this figure legend, the reader is referred to the web version of this article.)

**Table 1**
Properties of the Cambrian-Permian source rocks from the Sichuan Basin.

| Source rock | Lithology | Kerogen type | Thickness | TOC | Ro |
|---|---|---|---|---|---|
| Sinian Doushantuo Formation | Black carbonaceous shale, mudstone | Sapropelic | 20–220 m | 0.11 %–4.64 %, with an average of 1.51 % | 2.08 %–3.82 % |
| Cambrian Qiongzhusi Formation | Black carbonaceous shale, mudstone | Sapropelic | 60–500 m | 0.50 %–8.49 %, with an average of 1.94 % | 1.83 %–3.90 % |
| Silurian Longmaxi Formation | Black carbonaceous shale | Sapropelic | 30–120 m | 0.4 %–18.4 %, with an average of 2.5 % | 1.16 %–3.63 % |
| Lower Permian | Marlite | Sapropelic and Humic | 80–250 m | 0.5 %–1.5 %, with an average of 0.71 % | 1.79 %–2.45 % |
| Upper Permian Longtan Formation | Mudstone | Sapropelic and Humic | 20–170 m | 0.12 %–20.30 %, with an average of 2.61 % | 1.88 %–2.14 % |

**Table 2**
Information of the thermochronological samples.

| Sample | Strata | Lithology | Depth (m) |
|---|---|---|---|
| YF1–1 | $T_3$(235–201 Ma) | Drilling sandstone | 436 |
| YF1–2 | $O_1$(485–470 Ma) | Drilling sandstone | 2980 |
| YF1–3 | $\epsilon_1$(514–509 Ma) | Drilling sandstone | 4413 |

matter maturity and Ro (Sweeney and Burnham, 1990). The Ro values, Ro-depth gradients, and geothermal gradients during the Middle and Late Permian show an abrupt change (Fig. 2, Supplementary Table 2), suggesting that the geothermal field undergone significant changes cross the GLB.

One typical well's thermal history was reconstructed (Fig. 3). The Middle Permian Maokou Formation underwent denudation in the mid-late Guadalupian before to the Emeishan LIP(He et al., 2003; Liu et al., 2021). Based on the remnant thickness of the Maokou Formation, an estimate denudation of 500 m was set for the burial history of Well YF1. The Meso-Cenozoic denudation was constrained by the apatite fission track (AFT), apatite (U-Th)/He (AHe) and zircon (U-Th)/He (ZHe) data (Fig. 3b). The thermal histories of two samples (YF1–2 and YF1–3) at different depths were constrained by zircon fission track (ZFT) and ZHe data (Fig. 3c, d). The burial history was reconstructed by basin modeling (Fig. 3e). Based on the temperature paths and burial history, the paleotemperature gradient at 264, 259 and 254 Ma was 33, 42 and 35 °C/km, respectively (Fig. 3f). The thermal history indicated a lower heat flow value (56 mW/m$^2$) during the Early Paleozoic. The heat flow reached the maximum of 85 mW/m$^2$ at the end of the Middle Permian and then decreased rapidly to 67 mW/m$^2$ during the Late Permian (Fig. 3g). Recently, many studies have been carried out in the thermal history reconstruction of the Sichuan basin using paleothermal indicators, and thermal evolution since the Sinian was obtained (Feng et al., 2021; Jiang et al., 2018; Liu et al., 2018; Qiu et al., 2022; Zhu et al., 2010). The Sichuan Basin experienced the stable heat flow stage before the Early Permian, the rapid rising stage of heat flow in the end of the Early Permian, heat flow decline stage after the Late Permian. Here, we summarized the thermal history of the Sichuan Basin and reconstructed the thermal state of the Sichuan Basin at the mid-Permian (Supplementary Fig. 1). The peak heat flow is related to the distance from the center of the mantle plume. The southwest Sichuan basin near the center of the mantle plume has high anomalous heat flow values, but the peak heat flow is relatively low in the northeast Sichuan basin far from the mantle plume or has no effect.

**Table 4**
Zircon fission track data.

| Sample | Grain No. | ρs ($10^5$/cm$^2$) (Ns) | ρi ($10^5$/cm$^2$ (Ni) | ρd ($10^5$/cm$^2$) (Nd) | P ($\chi$2) | ZFT age (±1σ) (Ma) |
|---|---|---|---|---|---|---|
| YF1–3 | 34 | 157.691 (7549) | 44.661 (2138) | 13.396 (6949) | 0 | 205 ± 9 |

ρs, ρi and ρd are the density of spontaneous, induce and dosimeter tracks, respectively. Ns, Ni and Nd are the number of spontaneous, induce and dosimeter tracks, respectively. P($\chi^2$) is chi-square probability.

## 5. Discussion

### 5.1. Effect on fossil energy formation

Fossil energy (oil, gas, and coal) is carbon rich and is formed through organic matter enrichment followed by thermal evolution. The organic matter abundance determines the potential of fossil energy. TOC, an indicator of marine primary productivity, is the commonly used for evaluating organic matter abundance(Schoepfer et al., 2015). Volcanic activity brings many nutrients to the ocean surface, enhancing productivity and accumulating abundant organic matter in a short period, forming high-TOC source rock (Shen et al., 2015). Here, we present the Permian TOC records derived from 8 wells in the Sichuan Basin, showing that TOC has an abrupt change cross GLB (Fig. 4, Supplementary Table 1). The high spatial correspondence between TOC of the Wuchiapingian source rock (Fig. 1e) and the Emeishan basalt thickness (Fig.1c), suggests the Emeishan LIP likely triggered the Wuchiapingian organic carbon enrichment and coal ore genesis. The $\delta^{13}C$ records in Kamura, Japan and Verbit, Croatia at the GLB indicate an abnormally high marine primary productivity and the burial of abundant organic carbon in the Panthalassa region at low latitudes(Isozaki et al., 2007). The increase in atmospheric $CO_2$ and temperature and increased nutrient (e.g., Fe, Zn, and P) input, due to ash dispersal from subaerial eruptions and basalt weathering, created beneficial conditions for biological growth that, in turn, would lead to increased carbon burial and expanded anoxia in shallow waters (Clapham and Renne, 2019).

The organic matter maturity depends on the temperature and heating time. Several sets of hydrocarbon resource rocks (the Sinian, lower Cambrian, lower Silurian, and Permian) developed in the Sinian-Paleozoic in South China. The geological and geochemical characteristics of these source rocks are shown in the Table 1. Based on the burial thermal histories (Fig.3e, g), the maturity and temperature evolutions of Paleozoic source rocks in the Well YF1 (Fig.3h) were reconstructed. Due to the thermal effect of the LIP, the temperature in the Lower Cambrian exhibited a 120 °C rise, and the maturity increased from 0.8 % to 2.4 %

**Table 3**
Apatite fission track data.

| Sample | Grain No. | ρs ($10^5$/cm$^2$) (Ns) | U(ppm) | ζICP (±2σ) (yr cm$^2$) | P($\chi$2) | AFT age (±1σ) (Ma) | Mean track length (±SD) (μm) (number) | Dpar (μm) |
|---|---|---|---|---|---|---|---|---|
| YF1–1 | 40 | 36.95(1075) | 37.8 | 0.531 ± 0.058 | 0.3 | 48.2 ± 3.4 | 12.08 ± 1.79(21) | 1.6 |

$\zeta_{ICP}$ is the zeta factor for the ICP-MS. P($\chi^2$) is chi-square probability. SD is the standard deviation of measured confined track lengths.

**Table 5**
Apatite (U-Th)/He data.

| Sample | Grain | Radius (μm) | Mass (μg) | $^4$He (nmol▪g$^{-1}$) | U (ppm) | Th (ppm) | Sm (ppm) | eU (ppm) | FT | Corrected AHe age (±1σ) (Ma) |
|---|---|---|---|---|---|---|---|---|---|---|
| YF1–1 | A1 | 56.10 | 4.35 | 0.23 | 1.61 | 18.52 | 146.23 | 5.96 | 0.74 | 9.5 ± 0.5 |
| | A2 | 40.00 | 1.63 | 0.33 | 5.17 | 28.70 | 35.58 | 11.91 | 0.65 | 7.8 ± 0.6 |
| | A3 | 33.60 | 1.07 | 0.64 | 10.38 | 44.90 | 173.08 | 20.93 | 0.59 | 9.5 ± 0.5 |
| | A4 | 40.10 | 1.55 | 0.66 | 6.31 | 48.76 | 86.27 | 17.77 | 0.65 | 10.4 ± 0.6 |

**Table 6**
Zircon (U-Th)/He data.

| Sample | Grain | Radius (μm) | Mass (μg) | $^4$He (nmol▪g$^{-1}$) | U (ppm) | Th (ppm) | eU (ppm) | FT | Corrected AHe age (±1σ) (Ma) |
|---|---|---|---|---|---|---|---|---|---|
| YF1–1 | Z1 | 59.4 | 5.6 | 18.0 | 227.6 | 50.2 | 239.4 | 0.8 | 109.1 ± 6.8 |
| | Z2 | 46.2 | 3.6 | 29.8 | 448.2 | 180.3 | 490.5 | 0.7 | 135.5 ± 8.2 |
| YF1–2 | Z1 | 51.9 | 6.5 | 26.8 | 277.4 | 80.3 | 296.2 | 0.8 | 113.2 ± 7.0 |
| | Z2* | 62.3 | 9.2 | 33.8 | 37.5 | 23.1 | 43.0 | 0.8 | 656.1 ± 40.7 |
| | Z3 | 54.4 | 4.6 | 21.8 | 343.9 | 110.2 | 369.8 | 0.8 | 104.4 ± 6.5 |
| | Z4 | 60.8 | 5.8 | 23.4 | 223.9 | 30.1 | 230.9 | 0.8 | 142.9 ± 8.9 |
| | Z4 | 43.4 | 2.3 | 8.1 | 98.7 | 51.8 | 110.8 | 0.7 | 256.5 ± 15.9 |
| YF1–3 | Z1 | 59.2 | 5.5 | 1.7 | 92.3 | 205.4 | 140.6 | 0.8 | 17.9 ± 1.1 |
| | Z2 | 49.8 | 4.0 | 8.9 | 614.3 | 254.8 | 674.2 | 0.7 | 27.3 ± 1.7 |
| | Z3* | 61.1 | 6.2 | 13.3 | 223.8 | 14.1 | 227.1 | 0.8 | 76.5 ± 4.7 |
| | Z4 | 42.0 | 2.8 | 1.3 | 97.8 | 85.4 | 117.9 | 0.7 | 32.4 ± 2.0 |
| | Z5 | 39.7 | 2.8 | 1.1 | 202.6 | 119.3 | 230.6 | 0.7 | 14.6 ± 0.9 |

* Grains with significantly older ZHe ages have not been included in the inverse models.

within 5Myrs, indicating all liquid oil had been cracked into gas at the end-Guadalupian. The temperature in the Lower Silurian and Lower Permian increased by 90 °C and 80 °C respectively, and the maturity increased by~0.4 %.

### 5.2. Positive feedback to carbon-climate change

The massive gases emission during LIP (Fig. 1f) caused climate fluctuations, such as intensified land weathering, sharp temperature rises, ocean acidification, and hypoxia(Ganino and Arndt, 2009; Grasby et al., 2011; Penn et al., 2018; Svensen et al., 2004; Yang et al., 2018). The severity of volcanism-related environmental and biotic perturbations is positively correlated with the volume and rate of $CO_2$ emissions (Jiang et al., 2022). Here, we reconstructed the paleo-surface temperatures (the temperature at the sedimentary surface of the strata, a burial depth of 0 m) before, during, and after the eruption of the Emeishan LIP (Fig. 3f). Based on the temperature evolution paths and burial histories of two samples, the burial depths (1000 m and 2500 m) and

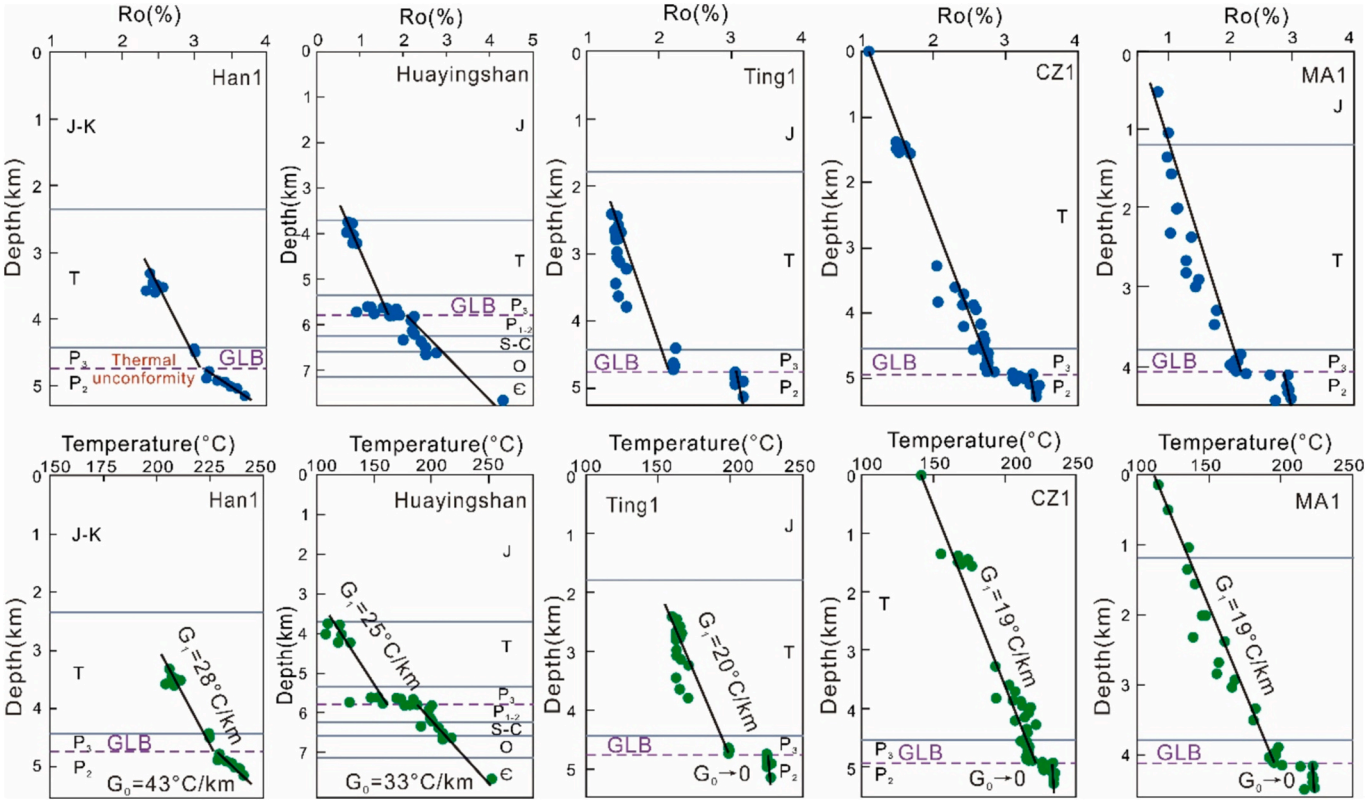


**Fig. 2.** Ro-depth and temperature-depth profiles of typical wells and outcrops in the Sichuan Basin. $G_0$ and $G_1$ represent the geothermal gradient during the Middle and Upper Permian.

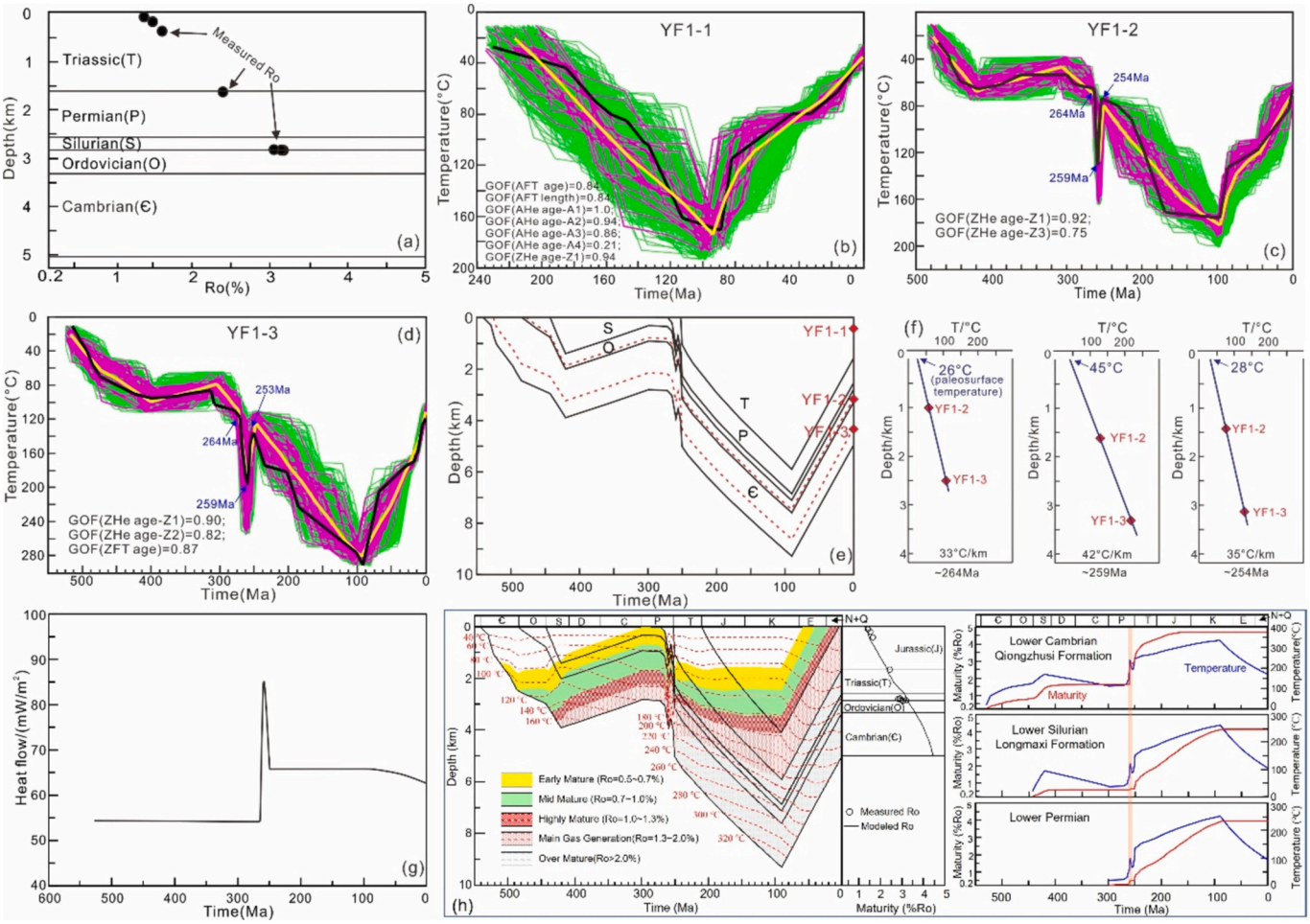


**Fig. 3.** Permian thermal pulse event. (a) Ro profile of Well YF1. (b) Thermal histories of sample YF1–1. The good-fit, acceptable, weighted mean and best-fit paths are within the purple, green, yellow and black lines, respectively. (c) Thermal histories of sample YF1–2. (d) Modeled thermal histories of sample YF1–3. (e) Burial history of Well YF1. The diamonds represent the thermochronology samples. The red dashed lines represent the burial histories of the two samples. (f) Paleo-temperature profiles showing the paleogeothermal gradients (33, 42, 35 °C/km) and paleosurface temperatures (26, 45, 28 °C) at 264, 259 and 254 Ma. (g) Thermal history of Well YF1. (h) The burial and thermal histories and simulated maturity of the Well YF1 and the temperature (blue lines) and maturity (red lines) evolution of the Paleozoic source rocks. (For interpretation of the references to colour in this figure legend, the reader is referred to the web version of this article.)

temperatures (60 °C and 110 °C) at 264 Ma were determined, yielding a paleo-geothermal gradient of 33 °C/km. Using this gradient, the paleo-surface temperature (burial depth of 0 m) was calculated to be approximately 26 °C. Similarly, the paleo-surface temperatures at 259 Ma and 254 Ma were calculated to be 45 °C and 28 °C, respectively. These results revealed a pulsating thermal anomaly event in the mid-Permian (264–254 Ma) showing a pre-LIP warming event (19 °C increase in 5Myr) followed by a rapid cooling stage (17 °C decrease in 5 Myr) across the GLB and into the early Wuchiapingian. Our results are consistent with previous studies. The rapid post-eruptive basaltic weathering and silicic volcanism of the Emeishan LIP likely amplified the $CO_2$ consumption effect of the equatorial continent silicate weathering by 1.8–2.5 times and caused atmospheric $pCO_2$ to decline below the pre-LIP levels, resulting in climate cooling, coincided with the onset of the last Permian glacial event(Yang et al., 2018). The $\delta^{18}O$ records of conodonts and brachiopod shells indicate a warming event, followed by a cool stage across the GLB (Isozaki et al., 2007; Wang et al., 2020).

LIPs significantly affect the global carbon cycle. Magmatic degassing and contact metamorphism of sediments resulted in massive $CO_2$ emissions. Monte Carlo simulations reveal that the $CO_2$ volume emitted from the Emeishan LIP (1.30 to 1.88 × $10^5$ Gt) is an order of magnitude as that of LIPs caused severe mass extinctions (Jiang et al., 2022). Mass balance modelling suggests that volcanic $CO_2$ was probably not the only trigger of carbon cycle perturbation (Wu et al., 2023). Large quantities of $^{13}C$-depleted carbon emissions from organic matter and $CH_4$ were likely required during complex interactions with volcanism. High-temperature $CH_4$ generated by geothermal anomalies is an important driver of the climate change and carbon cycle (Svensen et al., 2004; Chen et al., 2022). $CH_4$ is a powerful greenhouse gas with 25 times the global warming potential of $CO_2$ at a centennial time-scale(Sun et al., 2022). On a global scale, oil-cracked $CH_4$ emissions have likely contributed significantly to elevated $CH_4$ concentrations in the atmosphere in Earth's history as an important part of the global carbon cycle. In addition to the effect of global warming, $CH_4$, a reactive gas, is a precursor to other pollutants in the atmosphere (e.g., $CH_3C_1$) and significantly affects the biosphere (e.g., ozone depletion)(Black et al., 2014). The thermal metamorphism of Siberian coal measures and organic-rich shales led to $CH_4$ emissions, affecting the global climate and carbon cycling(Sobolev et al., 2011). We have demonstrated above that the Emeishan LIP thermal pulse event caused an increase from 0.8 % to 2.4 % of maturation of the Lower Cambrian source rock and liquid crude oil turned into pyrobitumen in the well YF1. Based on the total content of pyrobitumen and its yield, the total $CH_4$ emissions of the Cambrian source rock in the Sichuan basin were ~ 1440 Gt(Chen et al., 2022).The thermal anomalies (Supplementary Fig. 1) indicate that nearly 1/2 of the Lower Cambrian in the Sichuan Basin produced pyrobitumen at the end-Guadalupian. It can be concluded that the $CH_4$ of the Cambrian induced by the Emeishan LIP was ~720 Gt. Due to the deeper burial, the

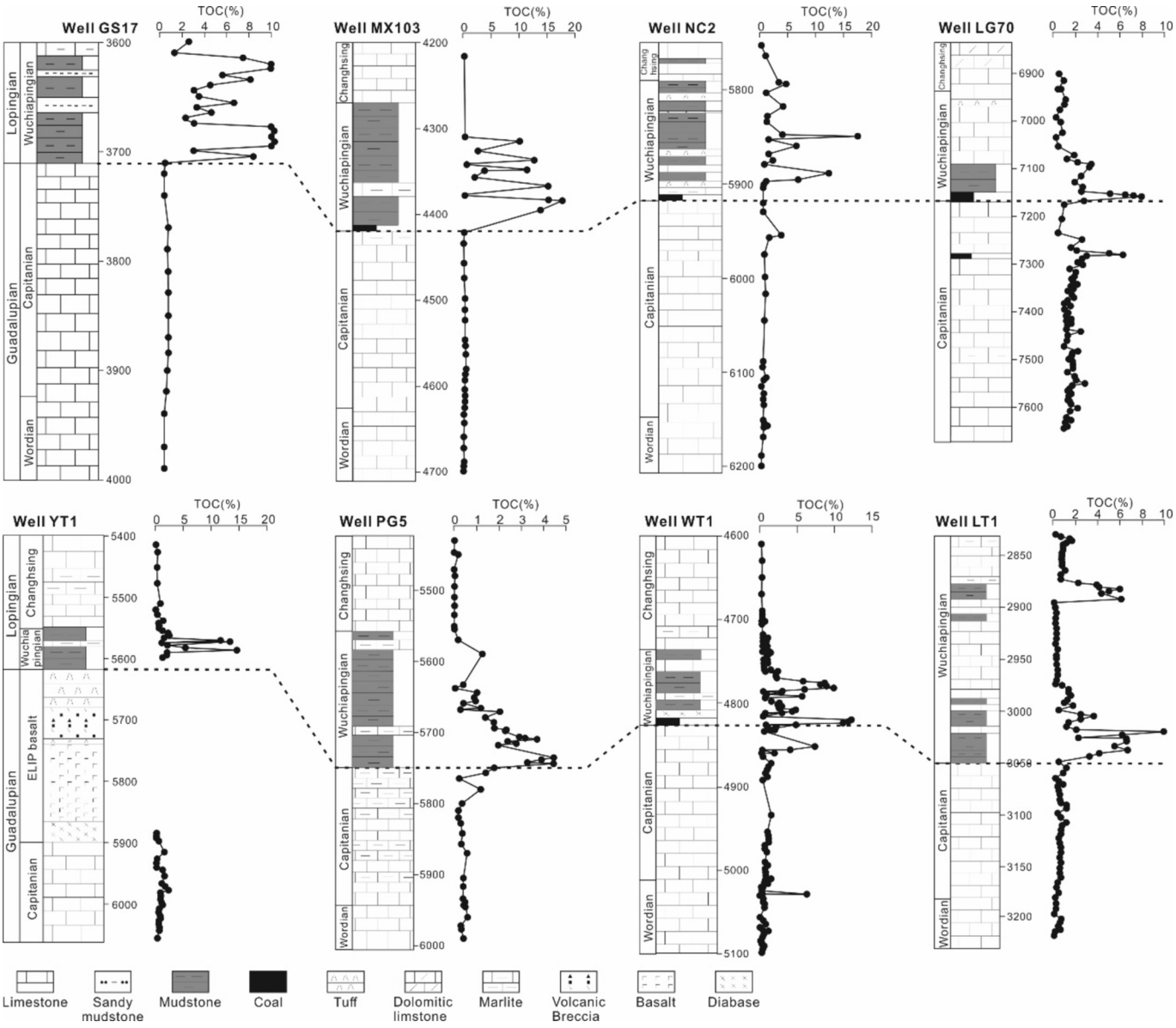


**Fig. 4.** Comparison of TOC contents of typical wells in the Sichuan Basin. The well locations are shown in Fig.1e.

thermal anomalies had a more significant effect on the maturation of the Sinian source rock. Moreover, the thermal effect range extends far 1/2 of the Sichuan Basin. Therefore, the $CH_4$ emissions caused by the Emeishan LIP was much greater than 1440 Gt. The mass of oil-cracked $CH_4$ equivalent to 40,410 Gt of $CO_2$ is nearly twice as large as the $CO_2$ volume released by the Emeishan LIP itself (16,800 Gt)(Ganino and Arndt, 2009), and more than one thousand times the annual global carbon emissions by human beings (e.g., 36 Gt of $CO_2$ emission in 2019)(IEA, 2021). It should be noted that the high-temperature methane generated by the thermal events is much greater than 1440 Gt, because the influence range of this thermal events extends far beyond half of the Sichuan Basin and there are other source rocks (i.e. the Sinian Dengying Formation, Silurian Longmaxi Formation), which would also produce large amounts of high-temperature $CH_4$.

The $\delta^{13}C$ records support the link between the thermal event induced by the LIP and the global carbon cycle. The $\delta^{13}C$ excursions across the GLB show two episodes (Fig. 5), which both occurred in the late Guadalupian and the early Lopingian. The biotic crises across the Ordovician-Silurian, Frasnian-Famenian, Permian-Triassic, and Triassic-Jurassic boundaries, are all characterized by two episodes of $\delta^{13}C$ changes (Shen et al., 2019; Racki et al., 2018; Xie et al., 2017; Hu et al., 2020). These four mass extinction events are associated with the Suordakh LIP, Karoo/Yakutsk-Vilyui LIP, Siberian Traps, and Central Atlantic Magmatic Province, respectively (Burgess and Bowring, 2015; Ernst and Youbi, 2017). We infer that carbon emissions during the LIP emplacement are characterized by a change of degassing style that, while continually varying, can be divided into phase 1 dominated by thermogenic carbon and phase 2 with volcanic $CO_2$-dominated (Fig. 6). Before massive basalt eruption, the contact metamorphism of sediments resulted in massive $CO_2$ emissions. The thermal event caused the rapid maturation of source rock and cracking of crude oil, which produced large amounts of $CH_4$. During magma erupts, magmatic degassing generates massive $CO_2$. It should manifest as a mixed volcanic and thermogenic carbon source during two phases, which is consistent with the carbon emission process simulated in the Earth system model (Wu et al., 2023). The $\delta^{13}C$ excursion in the Guadalupian suggests a $CO_2$ source with a pre-GLB thermogenic carbon isotopic signature. In contrast, the $\delta^{13}C$ excursions in the Lopingian has a post-GLB volcanic $CO_2$ source. The $\delta^{13}C$ excursion values and the $CO_2$ emissions in the two stages exhibit nearly identical secular trends.

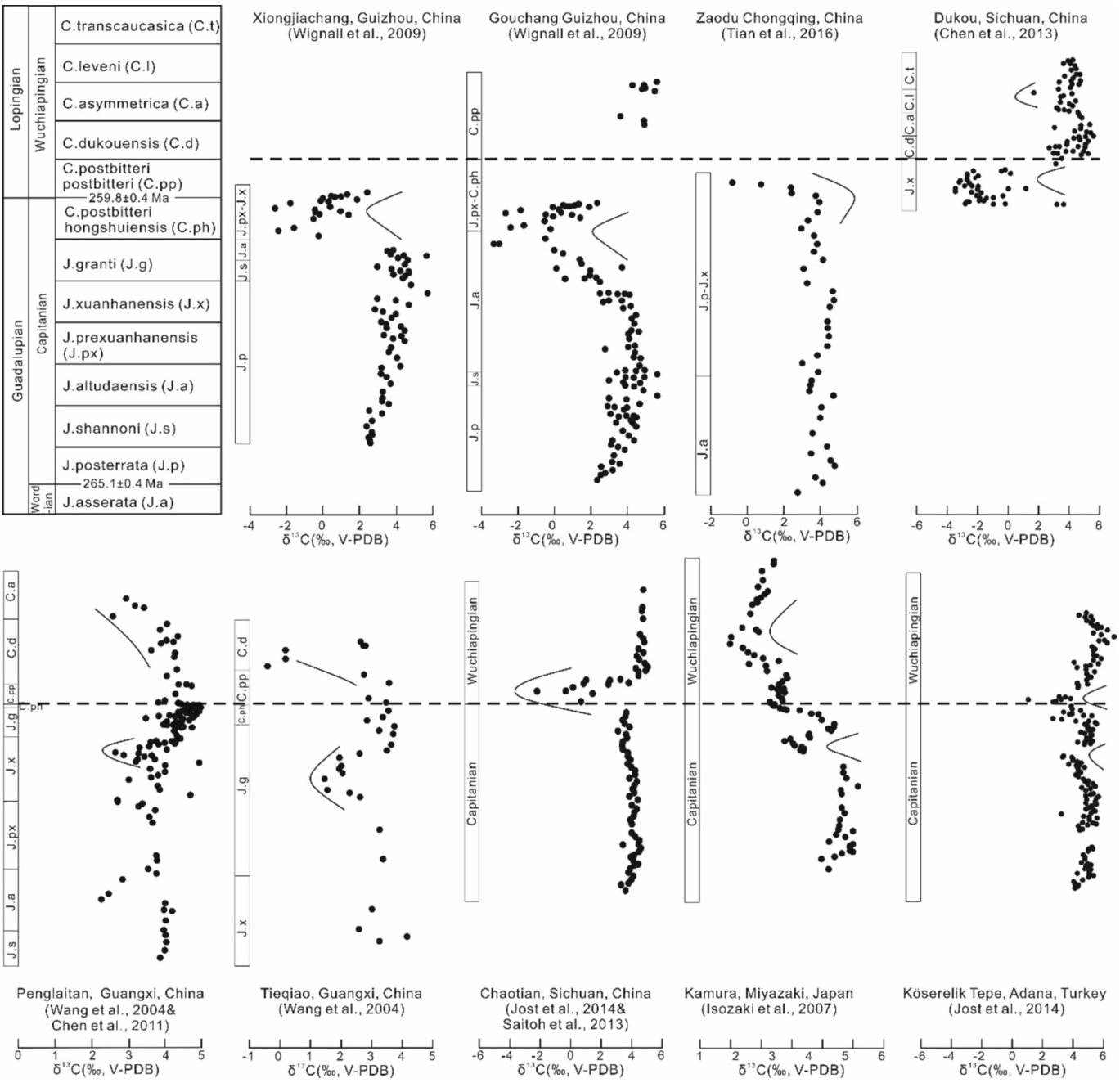


**Fig. 5.** Comparison of $\delta^{13}C$ chemostratigraphic results at the GLB. The conodont records are from Xiongjiachang, Gouchang(Wignall et al., 2009), Gouchang(Bond et al., 2010), Zaodu(Tian et al., 2016), Dukou(Shen et al., 2013), Penglaitian(Chen et al., 2011; Wang et al., 2004), Tieqiao(Wang et al., 2004), Chaotian(Jost et al., 2014; Saitoh et al., 2013), Köserelik Tepe(Jost et al., 2014), and Kamura(Isozaki et al., 2007).

## 6. Conclusions

In this study, geothermal evidences revealed the resource and environment effects of LIP. Southwestern China experienced a pulsating high thermal anomaly lasting 10 Mys during the mid-Permian, showing a pre-LIP warming event with a surface temperature increase of 19 °C, followed by a post-LIP cooling process (17 °C decrease). Emeishan LIP caused massive gases and volcanic ash emissions, which affected the Lopingain organic matter enrichment. The Permian pulsating thermal event accelerated the maturation and cracking of the lower Cambrian source rock across the GLB and produced large amounts of high-temperature $CH_4$. Carbon emissions during the LIP emplacement are characterized by a change of degassing style from the thermogenic source to volcanic $CO_2$, which contributed to two episodes of carbon changes across the GLB.

## CRediT authorship contribution statement

**Qianqian Feng:** Writing – review & editing, Writing – original draft, Resources, Methodology, Investigation, Data curation. **Nansheng Qiu:** Writing – review & editing, Writing – original draft, Methodology, Investigation, Funding acquisition, Conceptualization. **Xiongdong Fu:** Validation, Resources, Data curation. **Tenger Borjigin:** Supervision, Funding acquisition, Conceptualization. **Qingyong Luo:** Supervision, Software, Project administration. **Chuanqing Zhu:** Writing – review & editing.

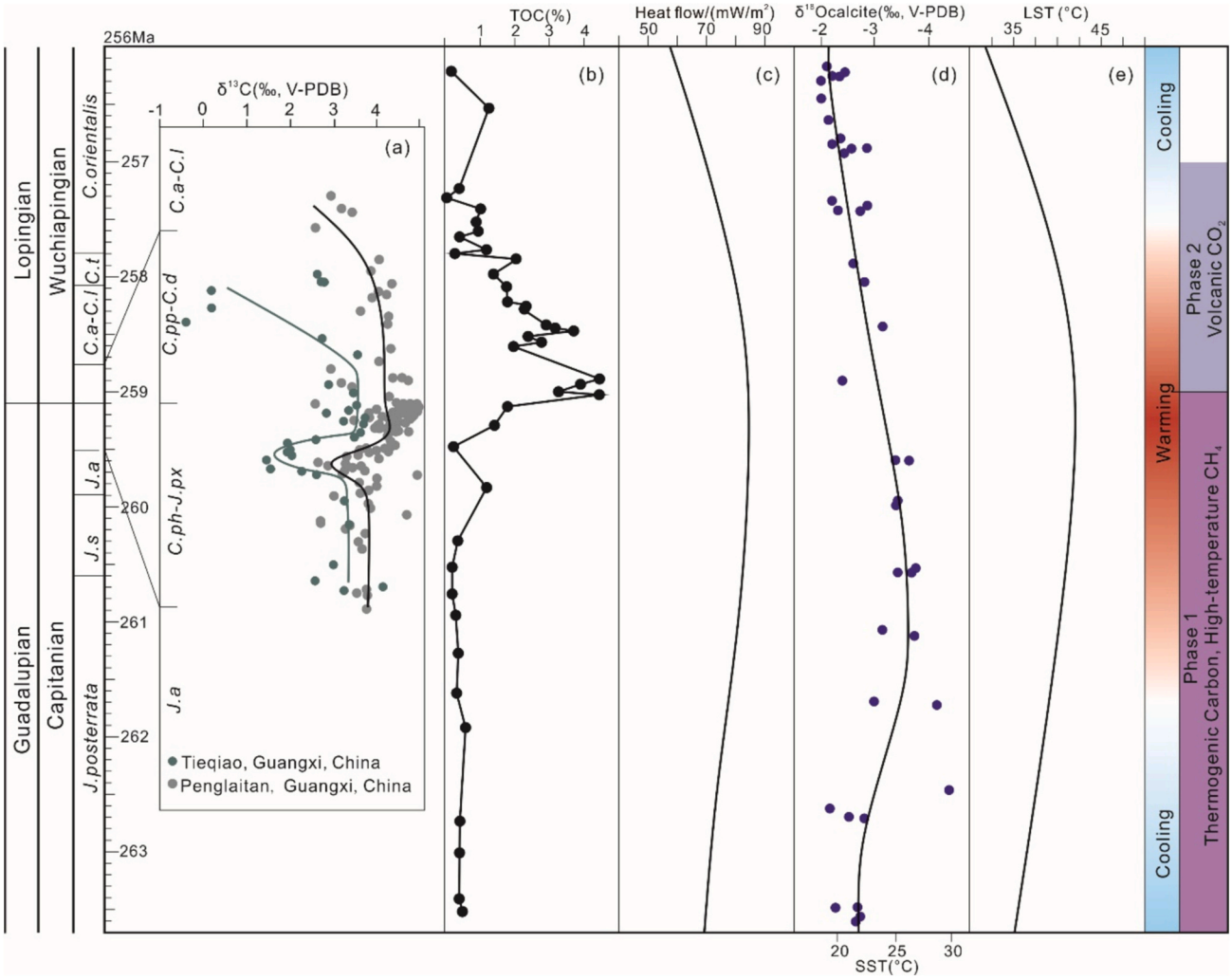


**Fig. 6.** Timeline across the GLB showing carbon isotopes, TOC, geothermal evolution, paleotemperature curves, and carbon emissions. (a) $\delta^{13}C$ records from Penglaitian and Tieqiao (Wang et al., 2004), showing carbon emissions during the LIP emplacement can be divided into phase 1 dominated by thermogenic source and phase 2 with volcanic $CO_2$-dominated. (b) TOC records from well PG5. (c) Thermal history. (d) $\delta^{18}O$ records and sea surface temperature (SST) curve (Wang et al., 2020). (e) Land surface temperature (LST) curve.

## Declaration of competing interest

The authors declare that they have no known competing financial interests or personal relationships that could have appeared to influence the work reported in this paper.

## Acknowledgements

This research has been funded by the National Natural Science Foundation of China (No. U2244208, 42302138) for financial support.

## Appendix A. Supplementary data

Supplementary data to this article can be found online at https://doi.org/10.1016/j.gloplacha.2025.104722.

## Data availability

We confirm that the data supporting the findings of this study are available within the study and the Supporting Information. The fission track, (U-Th)/He a data will eventually be deposited in the Mendeley Data repository by the time this article is accepted, and the data is available in the supporting information, tables, and figures for the purposes of peer review.

## References

Black, B.A., Lamarque, J., Shields, C.A., Elkins-Tanton, L.T., Kiehl, J.T., 2014. Acid rain and ozone depletion from pulsed Siberian Traps magmatism. Geology 42, 67–70. https://doi.org/10.1130/G34875.1.

Bond, D.P.G., Wignall, P.B., Wang, W., Izon, G., Jiang, H.S., Lai, X.L., Sun, Y.D., Newton, R.J., Shao, L.Y., Védrine, S., Cope, H., 2010. The mid-Capitanian (Middle Permian) mass extinction and carbon isotope record of South China. Palaeogeogr. Palaeoclimatol. Palaeoecol. 292, 282–294. https://doi.org/10.1016/j.palaeo.2010.03.056.

Burgess, S.D., Bowring, S.A., 2015. High-precision geochronology confirms voluminous magmatism before, during, and after Earth's most severe extinction. Sci. Adv. 1, e1500470. https://doi.org/10.1126/sciadv.1500470.

Chen, C.S., Qin, S.F., Wang, Y.P., Holland, G., Wynn, P., Zhong, W., Zhou, Z., 2022. High temperature methane emissions from Large Igneous Provinces as contributors to late Permian mass extinctions. Nat. Commun. 13, 6893. https://doi.org/10.1038/s41467-022-34645-3.

Clapham, M.E., Renne, P.R., 2019. Flood Basalts and Mass Extinctions. Annu. Rev. Earth Planet. Sci. 47, 275–303. https://doi.org/10.1146/annurev-earth-053018-060136.

Cogné, N., Chew, D.M., Donelick, R.A., Ansberque, C., 2020. LA-ICP-MS apatite fission track dating: A practical zeta-based approach. Chem. Geol. 531, 119302. https://doi.org/10.1016/j.chemgeo.2019.119302.

Ernst, R.E., Youbi, N., 2017. How Large Igneous Provinces affect global climate, sometimes cause mass extinctions, and represent natural markers in the geological record. Palaeogeogr. Palaeoclimatol. Palaeoecol. 478, 30–52. https://doi.org/10.1016/j.palaeo.2017.03.014.

Feng, Q.Q., Qiu, N.S., Fu, X.D., Li, W.Z., Xu, Q., Li, X., Wang, J.S., 2021. Permian geothermal units in the Sichuan Basin: Implications for the thermal effect of the Emeishan mantle plume. Mar. Pet. Geol. 132, 105226. https://doi.org/10.1016/j.marpetgeo.2021.105226.

Flowers, R.M., Ketcham, R.A., Shuster, D.L., Farley, K.A., 2009. Apatite (U-Th)/He thermochronometry using a radiation damage accumulation and annealing model. Geochim. Cosmochim. Acta 73, 2347–2365. https://doi.org/10.1016/j.gca.2009.01.015.

Ganino, C., Arndt, N.T., 2009. Climate changes caused by degassing of sediments during the emplacement of large igneous provinces. Geology 37 (4), 323–326. https://doi.org/10.1130/G25325A.1.

Grasby, S.E., Sanei, H., Beauchamp, B., 2011. Catastrophic dispersion of coal fly ash into oceans during the latest Permian extinction. Nat. Geosci. 4, 104–107. https://doi.org/10.1038/NGEO1069.

Guenthner, W.R., Reiners, P.W., Ketcham, R.A., Nasdala, L., Giester, G., 2013. Helium diffusion in natural zircon: radiation damage, anisotropy, and the interpretation of zircon (U-Th)/He thermochronology. Am. J. Sci. 313, 145–198.

He, B., Xu, Y.G., Chung, S.L., Xiao, L., Wang, Y.M., 2003. Sedimentary evidence for a rapid, kilometer-scale crustal doming prior to the eruption of the Emeishan flood basalts. Earth Planet. Sci. Lett. 213, 391–405. https://doi.org/10.1016/S0012-821X(03)00323-6.

He, L.J., 2022. Emeishan mantle plume and its potential impact on the Sichuan Basin: Insights from numerical modeling. Phys. Earth Planet. Inter. 54, 1948–1954. https://doi.org/10.1016/j.pepi.2022.106841.

Hu, F.Z., Fu, X.G., Lin, L., Song, C.Y., Wang, Z.W., Tian, K.Z., 2020. Marine Late Triassic-Jurassic carbon-isotope excursion and biological extinction records: New evidence from the Qiangtang Basin, eastern Tethys. Glob. Planet. Chang. 185, 103093. https://doi.org/10.1016/j.gloplacha.2019.103093.

Huang, B.C., Yan, Y.G., Piper, J.D.A., Zhang, D.H., Yi, Z., Yu, S., Zhou, T.H., 2018. Paleomagnetic constraints on the paleogeography of the East Asian blocks during Late Paleozoic and Early Mesozoic times. Earth Sci. Rev. 186, 8–36. https://doi.org/10.1016/j.earscirev.2018.02.004.

Huang, H., Huyskens, M.H., Yin, Q.Z., Cawood, P.A., Hou, M., Yang, J.H., Xiong, F.H., Du, Y.S., Yang, C.C., 2022. Eruptive tempo of Emeishan large igneous province, southwestern China and northern Vietnam: Relations to biotic crises and paleoclimate changes around the Guadalupian-Lopingian boundary. Geology 50, 1083–1087. https://doi.org/10.1130/G50183.1.

Hurford, A.J., Green, P.F., 1983. The zeta age calibration of fission track dating. Chem. Geol. 285–317. https://doi.org/10.1016/S0009-2541(83)80026-6.

IEA, 2021. World Energy Outlook 2021. IEA, Paris.

Isozaki, Y., Kawahata, H., Ota, A., 2007. A unique carbon isotope record across the Guadalupian–Lopingian (Middle-Upper Permian) boundary in mid-oceanic paleo-atoll carbonates: The high-productivity "Kamura event" and its collapse in Panthalassa. Glob. Planet. Chang. 55, 21–38. https://doi.org/10.1016/j.gloplacha.2006.06.006.

Jerram, D.A., Widdowson, M., Wignall, P.B., Sun, Y.D., Lai, X.L., Bond, D.P.G., Torsvik, T.H., 2016. Submarine palaeoenvironments during Emeishan flood basalt volcanism, SW China: implications for plume-lithosphere interaction during the Capitanian, Middle Permian ('end Guadalupian') extinction event. Palaeogeogr. Palaeoclimatol. Palaeoecol. 441, 65–73. https://doi.org/10.1016/j.palaeo.2015.06.009.

Jiang, Q., Qiu, N.S., Zhu, C.Q., 2018. Heat flow study of the Emeishan large igneous province region: Implications for the geodynamics of the Emeishan mantle plume. Tectonophysics 724-725, 11–27. https://doi.org/10.1016/j.tecto.2017.12.027.

Jiang, Q., Jourdan, F., Olierook, H.K.H., Merle, R.E., Bourdet, J., Fougerouse, D., Godel, B., Walker, A.T., 2022. Volume and rate of volcanic $CO_2$ emissions governed the severity of past environmental crises. Proc. Natl. Acad. Sci. 119 (31), e2202039119. https://doi.org/10.1073/pnas.2202039119.

Jiang, Q., Jourdan, F., Olierook, H.K.H., Merle, R.E., 2023. An appraisal of the ages of Phanerozoic large igneous provinces. Earth Sci. Rev. 237, 104314. https://doi.org/10.1016/j.earscirev.2023.104314.

Jost, A.B., Mundil, R., He, B., Brown, S.T., Altiner, D., Sun, Y.D., DePaolo, D.J., Payne, J.L., 2014. Constraining the cause of the end-Guadalupian extinction with coupled records of carbon and calcium isotopes. Earth Planet. Sci. Lett. 396, 201–212. https://doi.org/10.1016/j.epsl.2014.04.014.

Ketcham, R.A., Carter, A., Donelick, R.A., Barbarand, J., Hurford, A.J., 2007. Improved modeling of fission-track annealing in apatite. Am. Mineral. 92, 799–810. https://doi.org/10.2138/am.2007.2281.

Liu, W., Qiu, N., Xu, Q., Liu, Y., 2018. Precambrian temperature and pressure system of Gaoshiti-Moxi block in the central paleo-uplift of Sichuan Basin, southwest China. Precambrian Res. 313, 91–108.

Penn, J.L., Deutsch, C., Payne, J.L., Sperling, E.A., 2018. Temperature-dependent hypoxia explains biogeography and severity of end-Permian marine mass extinction. Science 362, 1130. https://doi.org/10.1126/science.aat1327.

Qiu, N.S., Chang, J., Zhu, C.Q., Liu, W., Zuo, Y.H., Xu, W., Li, D., 2022. Thermal regime of sedimentary basins in the Tarim, Upper Yangtze and North China Cratons, China. Earth-Sci. Rev. 224, 103884. https://doi.org/10.1016/j.earscirev.2021.103884.

Racki, G., Rakociński, M., Marynowski, L., Wignall, P.B., 2018. Mercury enrichments and the Frasnian-Famennian biotic crisis: a volcanic trigger proved? Geology 46, 543–546. https://doi.org/10.1130/G40233.1.

Saitoh, M., Isozaki, Y., Ueno, Y., Yoshida, N., Yao, J., Ji, Z., 2013. Middle–Upper Permian carbon isotope stratigraphy at Chaotian, South China: Pre-extinction multiple upwelling of oxygen-depleted water onto continental shelf. J. Asian Earth Sci. 67-68, 51–62. https://doi.org/10.1016/j.jseaes.2013.02.009.

Schoepfer, S.D., Shen, J., Wei, H., Tyson, R.V., Ingall, E., Algeo, T.J., 2015. Total organic carbon, organic phosphorus, and biogenic barium fluxes as proxies for paleomarine productivity. Earth Sci. Rev. 149, 23–52. https://doi.org/10.1016/j.earscirev.2014.08.017.

Self, S., Blake, S., Sharma, K., Widdowson, M., Sephton, S., 2008. Sulfur and chlorine in late Cretaceous Deccan magmas and eruptive gas release. Science 319, 1654–1657. https://doi.org/10.1126/science.1152830.

Shen, J., Schoepfer, S.D., Feng, Q.L., Zhou, L., Yu, J.X., Song, H.Y., Wei, H.Y., Algeo, T.J., 2015. Marine productivity changes during the end-Permian crisis and Early Triassic recovery. Earth Sci. Rev. 149, 136–162. https://doi.org/10.1016/j.earscirev.2014.11.002.

Shellnutt, J.G., Pham, T.T., Denyszyn, S.W., Yeh, M.W., Tran, T.A., 2020. Magmatic duration of the Emeishan large igneous province; insight from northern Vietnam. Geology 48, 457–461. https://doi.org/10.1130/G47076.1.

Shen, J., Algeo, T.J., Chen, J., Planavsky, N.J., Feng, Q.L., Yu, J.X., Liu, J.L., 2019. Mercury in marine Ordovician/Silurian boundary sections of South China is sulfide-hosted and non-volcanic in origin. Earth Planet. Sci. Lett. 511, 130–140. https://doi.org/10.1016/j.epsl.2019.01.028.

Shen, S., Cao, C., Zhang, H., Bowring, S.A., Henderson, C.M., Payne, J.L., Davydov, V.I., Chen, B., Yuan, D., Zhang, Y., Wang, W., Zheng, Q., 2013. High-resolution $\delta^{13}$Ccarb chemostratigraphy from latest Guadalupian through earliest Triassic in South China and Iran. Earth Planet. Sci. Lett. 375, 156–165. https://doi.org/10.1016/j.epsl.2013.05.020.

Shen, W.J., Sun, Y.G., Lin, Y.T., Liu, D.H., Chai, P.X., 2011. Evidence for wildfire in the Meishan section and implications for Permian-Triassic events. Geochim. Cosmochim. Acta 75, 1992–2006. https://doi.org/10.1016/j.gca.2011.01.027.

Sobolev, S.V., Sobolev, A.V., Kuzmin, D.V., Krivolutskaya, N.A., Petrunin, A.G., Arndt, N.T., Radko, V.A., Vasiliev, Y.R., 2011. Linking mantle plumes, large igneous provinces and environmental catastrophes. Nature 477, 312–316. https://doi.org/10.1038/nature10385.

Sun, F.N., Hu, W.X., Cao, J., Wang, X.L., Zhang, Z.R., Ramezani, J., Shen, S.Z., 2022. Sustained and intensified lacustrine methane cycling during Early Permian climate warming. Nat. Commun. 13, 4856. https://doi.org/10.1038/s41467-022-32438-2.

Svensen, H., Planke, S., Malthe-Sorenssen, A., Jamtveit, B., Myklebust, R., Rasmussen, E.T., Rey, S.S., 2004. Release of methane from a volcanic basin as a mechanism for initial Eocene global warming. Nature 429, 542–545. https://doi.org/10.1038/nature02566.

Sweeney, J.J., Burnham, A.K., 1990. Evaluation of a Simple Model of Vitrinite Reflectance Based on Chemical Kinetics. AAPG Bull. 70, 1559–1570. https://doi.org/10.1306/0C9B251F-1710-11D7-8645000102C1865D.

Tian, X.S., Shi, Z.J., Yin, G., Long, H.Y., Wang, K., 2016. A correlation between the Large Igneous Provinces and mass extinctions: constraint on the end-Guadalupian mass extinction and the Emeishan LIP in South China, eastern Tethys. Int. Geol. Rev. 58, 1215–1233. https://doi.org/10.1080/00206814.2016.1147384.

Wang, W., Cao, C.Q., Wang, Y., 2004. The carbon isotope excursion on GSSP candidate section of Lopingian-Guadalupian boundary. Earth Planet. Sci. Lett. 220, 57–67. https://doi.org/10.1016/S0012-821X(04)00033-0.

Wang, W.Q., Garbelli, C., Zhang, F.F., Zheng, Q.F., Zhang, Y.C., Yuan, D.X., Shi, Y.K., Chen, B., Shen, S.Z., 2020. A high-resolution Middle to Late Permian paleotemperature curve reconstructed using oxygen isotopes of well-preserved brachiopod shells. Earth Planet. Sci. Lett. 540, 116245. https://doi.org/10.1016/j.epsl.2020.116245.

Wignall, P.B., Sun, Y., Bond, D.P.G., Izon, G., Newton, R.J., Védrine, S., Widdowson, M., Ali, J.R., Lai, X., Jiang, H., Cope, H., Bottrell, S.H., 2009. Volcanism, Mass Extinction, and Carbon Isotope Fluctuations in the Middle Permian of China. Science 324, 1179–1182. https://doi.org/10.1126/science.1171956.

Wu, Y.Y., Cui, Y., Chu, D.L., Song, H.J., Tong, J.N., Dal Corso, J., Ridgwell, A., 2023. Volcanic $CO_2$ degassing postdates thermogenic carbon emission during the end-Permian mass extinction. Sci. Adv. 9, eabq4082. https://doi.org/10.1126/sciadv.abq4082.

Xie, S.C., Algeo, T.J., Zhou, W.F., Ruan, X.Y., Luo, G.M., Huang, J.H., Yan, J.X., 2017. Contrasting microbial community changes during mass extinctions at the Middle/Late Permian and Permian/Triassic boundaries. Earth Planet. Sci. Lett. 460, 180–191. https://doi.org/10.1016/j.epsl.2016.12.015.

Xu, Y.G., He, B., Chung, S.L., Menzies, M.A., Frey, F.A., 2004. Geologic, geochemical, and geophysical consequences of plume involvement in the Emeishan flood-basalt province. Geology 32, 917–920. https://doi.org/10.1130/G20602.1.

Yamada, R., Murakami, M., Tagami, T., 2007. Statistical modelling of annealing kinetics of fission tracks in zircon; Reassessment of laboratory experiments. Chem. Geol. 236, 75–91. https://doi.org/10.1016/j.chemgeo.2006.09.002.

Yang, J.H., Cawood, P.A., Du, Y.S., Condon, D.J., Yan, J.X., Liu, J.Z., Huang, Y., Yuan, D.X., 2018. Early Wuchiapingian cooling linked to Emeishan basaltic weathering? Earth Planet. Sci. Lett. 492, 102–111. https://doi.org/10.1016/j.epsl.2018.04.004.

Zhang, G.J., Zhang, X.L., Li, D.D., Farquhar, J., Shen, S.Z., Chen, X.Y., Nan, S.Y., 2015. Widespread shoaling of sulfidic waters linked to the end-Guadalupian (Permian) mass extinction. Geology 43, 1091–1094. https://doi.org/10.1130/G37284.1.

Zhu, C.Q., Xu, M., Yuan, Y.S., Zhao, Y.Q., Shan, J.N., He, Z.G., Tian, Y.T., Hu, S.B., 2010. Palaeo-geothermal response and record of the effusing of Emeishan basalts in Sichuan basin. Chin. Sci. Bull. 55, 474–482. https://doi.org/10.1007/s11434-009-0490-y.